Fluid Topology in Drainage and Imbibition: Pore Scale Imaging by Synchrotron Tomography

Hamid Hosseinzade Khanamiri, Ole Torsæter, Georg J. B. Voss

PoreLab Research Center, Department of Geoscience and Petroleum, Norwegian University of Science and Technology (NTNU), 7491 Trondheim, Norway

This paper was prepared for presentation at the International Symposium of the Society of Core Analysts held in Vienna, Austria, 27 August – 1 September 2017.

ABSTRACT

Recent works on the enhanced oil recovery (EOR) by injection of low salinity surfactant (LSS) have shown that the efficiency of LSS can be sensitive to subtle changes in ionic composition. Different compositions can result in different interfacial tension (IFT), relative permeability, wettability and mobilization of residual oil. A flooding experiment including drainage and imbibition by water and LSS was performed on water-wet Berea sandstone. The 3-dimensional (3D) pore scale changes of the fluid configuration were captured under flow using fast X-ray tomography. The connectivity (Euler characteristic) was calculated separately for ganglia and for connected pathways of the wetting and nonwetting phases to give more insight of their impact on topology of the water and oil phases. The results showed that the topology of a fluid mainly depended on the topology of the corresponding ganglia and was less sensitive to topology of the corresponding connected pathway. The ganglia and the whole phase (ganglia plus connected pathway) showed hysteresis in the topology in imbibition and drainage for both wetting and nonwetting phases. The connected pathways however had insignificant hysteresis in imbibition and drainage, i.e. the hysteresis in topology of a phase was likely to be caused by the ganglia. Furthermore, we hypothesized that the ratio of the Euler characteristic of the connected pathways of wetting and of nonwetting phases could be used as a descriptor of the wetting change.

INTRODUCTION

In two-phase flow in porous media, nonwetting fluid moves either as a connected pathway or as a group of disconnected clusters (ganglia) which break up and coalesce (Avraam and Payatakes, 1995). The phenomenon where the disconnected clusters of the nonwetting phase are mobile is known as the ganglion dynamics. Synchrotron tomography has helped to understand better behavior of flowing fluids. Youssef et al. (2014) found that mean ganglia size and largest cluster size depend on capillary number. Rücker et al. (2015) observed that ganglion dynamics occurred at length scale equivalent to oil clusters length. Therefore, an intermediate flow regime between pore and Darcy scale is expected. Berg et al. (2015) showed that at the onset of oil mobilization, oil clusters break off as opposed to moving in the form of a single large cluster. One of the major challenges has been to find

a parameter which helps quantifying the dynamic microscopic changes. In this regard, Herring et al. (2013) used Euler characteristic (χ) to describe the connectivity of the oil clusters where χ is defined as:

$$\chi = N - L + O \quad (1)$$

In this equation, N is the number of isolated clusters of a fluid phase, L is the number of redundant connections within all clusters, and O is the number of cavities. A negative value of χ indicates higher connectivity while a positive value indicates fragmented fluid. χ is dimensionless; however it is usually normalized with the total volume of the system (bulk volume) for convenience. We have reported the normalized values in mm^{-3} unit. Schlüter et al. (2016) believed that the connectivity had been ignored in characterization of two-phase flow. Avraam and Payatakes (1995) observed a dependency of relative permeabilities on changes in microscopic flow regimes when the flow regime changes from ganglion dynamics to connected pathway. Relative permeability depends on pore scale fluid configuration which in turn, depends on the connectivity (Armstrong et al. 2017). Overall, recent advances seem to be promising for better understanding of two-phase flow.

In this work, we examined the drainage and imbibition in a water wet Berea sandstone sample. The connectivity was calculated for both water and oil phases. In addition, the connectivity of the oil and water ganglia, and of the oil and water connected pathways were calculated separately. The evolution of ganglia and connected pathways topology revealed their effect on the connectivity of the whole phases and on the origins of connectivity hysteresis.

MATERIALS AND METHODS

Material. The core sample was a Berea sandstone (D=4mm, L≈10mm) extracted from a parent plug which had a permeability and porosity of 270mD and 15.2%, respectively. There was no aging before the experiment. The composition of the brines is given in Table 1. The core was initially saturated with high salinity water (HSW). The ionic strength of low salinity water (LSW) was 10 times lower than that of the HSW. LSW-N contains only NaCl and LSW-NC contains both NaCl and $CaCl_2$ in the solution. The low salinity surfactant (LSS) solutions were prepared by dissolving 0.5 wt% surfactant in the LSW-N and LSW-NC. LSS-N and LSS-NC are the surfactant solutions which were prepared using LSW-N and LSW-NC brines, respectively. The surfactant is a blend of alkylbenzene sulfonates with a chain length distribution of C_{15}-C_{18} (Khanamiri et al. 2016a, b). Detailed properties of the surfactant can be found in the aforementioned references. The oil phase was a mixture of 90% by volume crude oil and 10% 1-Iododecane. 1-Idododecane enhances the contrast of oil and water phases. The oil phase was used in a previous study by Khanamiri et al. (2016b) where the crude oil properties were also documented. IFT of the mixed oil with the HSW, LSS-N, LSS-NC were 5.3, 0.1 and 0.03mN/m, respectively at room temperature.

Injection and imaging. The experiment was conducted at ambient conditions in the *TOMCAT* beamline at the *Swiss Light Source*. Details of the injection steps are listed in

Table 2. The core sample was 100% saturated with HSW (Table 1) before starting the experiment. Drainage was performed at two different flow rates. Waterflooding was done by HSW at two different flow rates. Low salinity surfactant (LSS) was then injected in four different steps denoted by LSS1-NC, LSS2-N, LSS3-NC and LSS4-N. LSS-N is the LSS with NaCl only and the LSS-NC is the one with both NaCl and $CaCl_2$ (See Table 1). The X-ray tomography was performed during the injections. The imaging in one scan took about 18 sec and the time interval between two scans was approximately two minutes. The pixel size of the projections was 3.25μm and the vertical field of view for camera was 2866μm. The number of scans per injection step is shown in the last column of Table 2.

Table 1: composition of the brines and surfactant solutions

Brine	NaCl [g/l]	$CaCl_2.2H_2O$ [g/l]	$MgCl_2.6H_2O$ [g/l]	$^*M^{2+}/M^+$	ionic strength [mol/l]
HSW	29.250	2.210	0.305	0.033	0.5561
LSW-N	3.25	-	-	0	0.0556
LSW-NC	3.202	0.0404	-	0.005	0.0556
LSS-N	0.5 wt% surfactant dissolved in LSW-N				
LSS-NC	0.5 wt% surfactant dissolved in LSW-NC				

$^*M^{2+}/M^+$ is the molar ratio of divalent to monovalent cations.

Table 2: details of injection and image acquisition

injection step	injection	flow rate (ml/min)	duration (≈min)	*PVI	scan No.
1	Oil injection 1	0.004	35	7	1-18
2	Oil injection 2	0.04	10	20	19-23
3	HSW1	0.004	15	3	24-31
4	HSW2	0.008	15	6	32-39
5	LSS1-NC	0.008	20	8	40-49
6	LSS2-N	0.008	20	8	50-58
7	LSS3-NC	0.008	20	8	59-69
8	LSS4-N	0.008	20	8	70-81

* **PVI** was the injected volume in terms of number of pore volume of the whole core. The pore volume of the core with 10mm length was roughly 0.02ml.

Image Processing. The reconstruction of 3D tomographic data sets from 2D projections was obtained during the injection experiment using *ImageJ*. The analyzed height was 2447μm and the analyzed volume was about 964 million voxels in each model. The images were denoised by an anisotropic diffusion filtering (Tschmperlé and Deriche 2005) which is an effective denoising technique that preserves edges. The filtering was implemented in *Xlib* plugin (Münch 2015) of *ImageJ*. Statistical Region Merging (Nock and Nielsen 2004) was used for segmentation. Afterwards, the moment-preserving thresholding (Tsai 1985) was used to segment the water phase and the *Default* thresholding method in *ImageJ* was used to extract the pore volume. The oil phase was then obtained by subtracting the water images from pore volume images. As a cleaning cut-off, any object smaller than 3^3 voxel was removed from the 3D models. The largest cluster in each 3D data set of oil was assumed to be the oil connected pathway and the rest of the clusters were considered the oil ganglia. Water phase was also treated in the same manner. The 3D size analysis of oil clusters was obtained in *CTAn*. The phase volume and Euler characteristic were calculated using *BoneJ* plugin (Doube et al. 2010) in *ImageJ*.

RESULTS AND DISCUSSION

The largest oil cluster was considered the oil connected pathway and the rest of the clusters were assumed to be the oil ganglia. The same assumption was made for the water phase. The total phase is therefore the summation of the connected pathway and ganglia. χ_{oT}, χ_{oG}

and χ_{oP} are the Euler characteristic of the total oil phase, oil ganglia and oil connected pathway, respectively. χ_{wT}, χ_{wG} and χ_{wP} denote the Euler characteristic of the total water phase, water ganglia and water connected pathway, respectively. The temporal resolution was 2 *min*.

Source of topological hysteresis in imbibition and drainage. The Euler characteristics of the total oil phase (χ_{oT}) vs S_w at high salinity water (HSW) injection is different from that at drainage, as shown in Figure 1. Therefore χ_{oT} might have a hysteretic behavior at drainage and imbibition processes. χ_o for the pathway and ganglia of the oil phase were calculated and plotted separately to investigate the effect of ganglion dynamics and connected pathway on the hysteresis of the oil phase connectivity. As shown in Figure 1, hysteresis is apparent in χ_{oG} of the oil ganglia vs water saturation. χ_{oG} is similar to χ_{oT}. However, the connected pathway does not show hysteresis in drainage and imbibition; i.e. cause of the hysteresis in χ_{oT} for the total oil phase is the ganglia part of the phase. In the case of the wetting phase (water), χ_{wG} and χ_{wT} are also similar. Although the data seem more scattered, it still seems that there is also some hysteresis in χ_w between drainage and imbibition for the water ganglia (χ_{wG}) and the total water phase (χ_{wT}). Similar to the oil connected pathway, the water connected pathway has nearly no hysteresis in drainage and imbibition. Therefore, the hysteresis in connectivity (topology) of both the wetting and nonwetting phases in drainage and imbibition could be caused by the ganglia part of each phase. The creation or breakage of redundant connections is likely to be the main cause of topology change in the connected pathways. On the other hand, a broader range of events including snap-off, Hains jumps, redundant connections and coalescence change the topology of the ganglia. As a result, the topology of the ganglia resembles that of the total phase where all possible events collaborate in changing the topology (See Figure 1).

Euler characteristic of the nonwetting and wetting phases. The ranges of χ for the wetting and nonwetting phases are slightly different. The redundant connections of the connected pathway could be more stable in the wetting phase i.e. they may not break easily as they have strong contact with the rock grains. Therefore, further creation or disappearance of the redundant connections could be minimized. On the other hand, connected pathway in the nonwetting phase (oil) most likely creates connections frequently with the numerous clusters of the oil ganglia. In other words, topology of water connected pathway could evolve mainly by *film flow*/*film expansion* while topology of oil connected pathway could evolve mainly by *jump-and-coalescence*. These changes could explain that larger topological variations in the nonwetting connected pathway occur than in the wetting connected pathway (See Figure 1).

Euler characteristic is an additive function. This means that adding χ_{oP} to χ_{oG} results in χ_{oT}; and adding χ_{wP} to χ_{wG} results in χ_{wT}. χ_{oP} and χ_{wP} are both negative, with χ_{oP} representing larger absolute values. Figure 1 shows also that χ_{oG} is larger than χ_{wG} (S_w≈0.51–0.73). Therefore χ_{oT}, on average, is larger than χ_{wT}; and nonwetting phase is in general more disconnected than the wetting phase (S_w≈0.51–0.73). However, the nonwetting phase is slightly more connected when S_w<0.51.

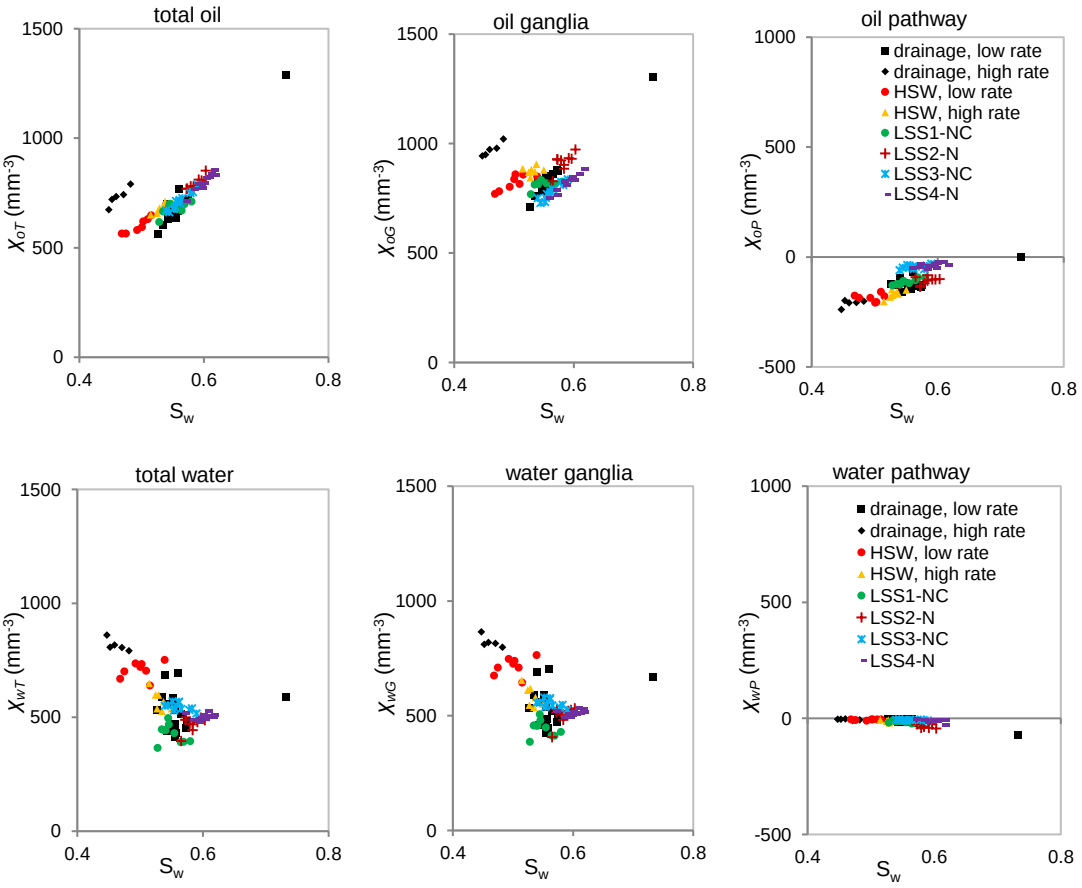

Figure 1: Euler characteristic of water and oil phases for the total phase (ganglia plus connected pathway), ganglia and connected pathway.

Pore geometry and topology of the wetting connected pathway. As mentioned in previous section, the total water phase is more connected than the total oil phase in the S_w interval of 0.51–0.73. It is also clear that the connected water pathway has near-zero negative χ_{wP} values while the connected pathway of the oil phase has higher connectivity. This may be caused by the presence of water in smaller pores and channels where oil phase is usually not present. Therefore, water could be trapped and isolated in smaller pores where the nonwetting oil phase would usually have little or no access. In other words, the topology of the wetting connected pathway may be dictated by the geometry of the porous media which is fixed and static. This discussion implies that it is a possibility to link the topological changes of the wetting connected pathway (χ_{wP}) to the possible wettability changes. The reason could be that topology of the connected pathway of water due to its affinity to rock may not change much unless the affinity itself has changed. This is discussed in detail later. On the other hand, it also suggests that the topology of the nonwetting phase is mainly affected by the process (drainage, imbibition, Figure 1) and the dynamics (rate changes, Figure 1) because it may be less affected by pore geometry compared to the wetting phase. Therefore, the topology of the nonwetting phase may describe the process better than that of the wetting phase can. For this reason, the recent

works have mainly focused on the topology of the nonwetting phase to study the pore scale phenomena (Schlüter et al. 2016, Rücker et al. 2015, Armstrong et al. 2016).

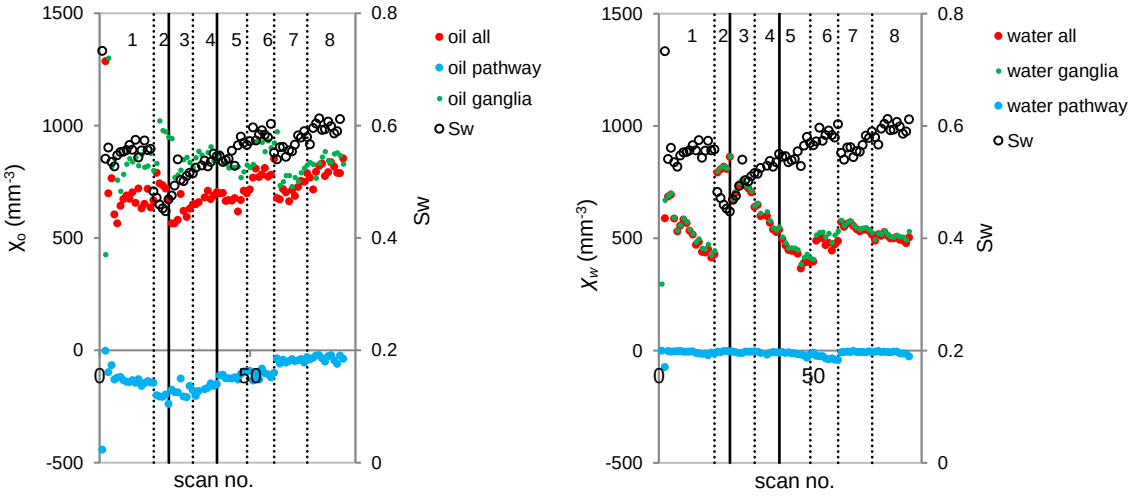

Figure 2: Evolution of χ for oil (*left*) and water (*right*) phases for the whole phase (all), ganglia and connected pathway; χ (*left vertical axis*) is shown by red, green and blue circles. S_w (*right vertical axis*) is shown by open circles. The numbers 1-8 represent the injection steps mentioned in **Table 2**.

Euler characteristic vs time and its reproducibility. Here, the evolution of topology and S_w vs time is discussed. The difference between χ_{wG} and χ_{wT} is insignificant while there is some difference between χ_{oG} and χ_{oT} (Figure 2). The connected pathway of oil becomes closer to the threshold of major fragmentation ($\chi_{oP}=0$) at the start of injection step 7 (third surfactant injection, LSS3-NC) and continues flowing under similar condition in steps 7 and 8 (LSS3-NC and LSS4-N); simultaneously χ_{oG} approaches χ_{oT}.

There is a reduction in S_w at injection step 7 (LSS3-NC), due to oil mobilization upstream of field of view of camera. S_w in step 7 is similar to that in step 5 (See Figure 2). S_w profiles of steps 6 and 8 are also similar. Therefore, it became possible to observe the changes in topology when the S_w history is repeated in surfactant injection. Figure 1 and Figure 2 show that χ_{oT} (oil phase) is almost reproducible in the mentioned injection steps and χ_{oG} (oil ganglia) have minor similarity in these two periods. On the other hand, χ_{wT} (water phase) and χ_{wG} (water ganglia) are different both in value and in trend. For the total nonwetting phase, Schlüter et al. (2016) also stated that the topology depends mainly on the process, not on the system history. The main reason would be the stronger dependency of the wetting phase connected pathway topology on the pore geometry and/or wetting and less dependency of nonwetting phase topology on those parameters, as discussed in the previous section. In case of the connected pathways, χ is not reproducible before and after invasion of upstream oil in neither of the water and oil phases.

IFT, wetting and ionic composition. Here, the implication of surfactant and ionic composition is discussed. Figure 3 shows no immediate change in number of oil clusters after switching to surfactant injection in step 5 (IFT 0.03mN/m). However, the number of

oil clusters almost in the middle of step 5 starts to increase. This could be a sign of oil solubilization by the surfactant. As shown in Figure 2 and Figure 3, χ_o for the total oil phase, oil ganglia and connected pathway of oil level off in step 5 for a short time after which they start increasing when the number of oil clusters starts increasing. Switching the surfactant injection to step 6 (IFT 0.1mN/m) with NaCl as the only salt in the injected solution causes a sharp increase in the number of oil clusters, χ_{oT} and χ_{oG}. Time resolution of 2 *min* is not sufficient to resolve the dynamics seconds after the composition change, but the outcome of the composition change is visible in the mentioned parameters. Smooth increase in S_w (See Figure 2) suggests that the observed behavior in step 6 is probably not due to possible oil mobilization upstream out of the field of view of the camera. The sharp increase in the number of oil clusters and χ_{oT} by switching from LSS-NC (IFT 0.03mN/m) to LSS-N (IFT 0.1mN/m) is also accompanied by a sharp increase in the χ_{wT} and χ_{wG} (See Figure 2 and Figure 3). An opposite behavior was observed for the connected pathway of the water phase. The increase in χ_w is the most obvious change for the connected pathway of water since start of the entire experiment. The change in the topology of the rather stable connected water pathway can be a result of the possible change in the wettability. Step 6 (LSS2-N) is the first step in the entire imbibition without $CaCl_2$ in the injected solution. In a previous work with the same rock type/oil/brine/surfactant system at similar wetting conditions of strongly water wet (Khanamiri et al. 2016b), we observed that low salinity surfactant with only NaCl (LSS-N) changed the wetting to less water wet more than the surfactant solution with both sodium and calcium cations did (LSS-NC). It seems that the ratio of Euler characteristic in the connected pathways of water and oil (χ_{wP}/χ_{oP}) could be used to qualitatively track changes of wettability (See Figure 4). Before surfactant injection, χ_{wP}/χ_{oP} is between 0 and 0.1. Afterwards it starts to variate sharply in surfactant injections with different ionic compositions.

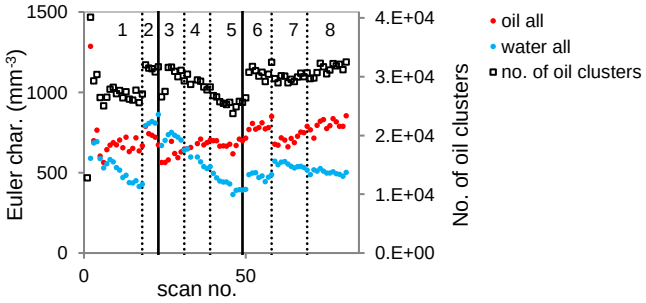

Figure 3: Changes in no. of oil clusters (*black markers/right vertical axis*) are similar to changes in χ_{wT}.

The hypothesis of using χ_{wP}/χ_{oP} to describe the wetting change should be examined by further experiments. The major observation is that changing the ionic composition in the surfactant injection does change the connectivity of the oil and water phases. Bartels et al. (2017a) found that the wetting changes in low salinity water injection led to the fragmentation and reconnection of oil in different pores. In another work, Bartels et al. (2017b) believed that the disconnection and reconnection of oil are characteristic of the ganglion dynamics. However, it is not possible to decide if the fragmentation/connection is driven by ganglion dynamics, the possible wetting change or both. We believe that the

topology of connected pathways, particularly in wetting phase, largely depends on the pore geometry and wetting. Since the pore geometry is fixed, the changes in topology of the connected pathways could be due to the wetting change.

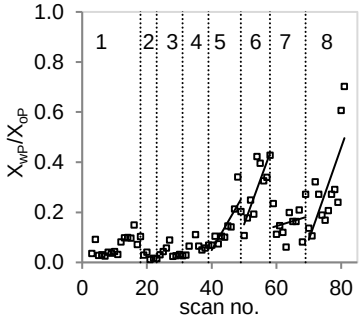

Figure 4: Ratio of the Euler characteristic for connected pathways of water and oil (χ_{wP}/χ_{oP}) vs time varies with varying ionic composition of the injected surfactant (steps 5-8). Four trend lines indicate the sharper changes at steps 6 & 8 (only NaCl) than at steps 5 & 7 (both NaCl & $CaCl_2$). This could be a sign of wetting change.

CONCLUSIONS

In an unsteady state two-phase immiscible flow experiment and by analyzing topology of the ganglia and connected pathways separately, we learned the following.

- The pore scale topology of fluids in two-phase displacement may be determined mainly by the topology of the ganglia, and appears less affected by the topology of the connected pathways.
- The ganglia and the whole phase (ganglia plus connected pathway) show hysteresis in the topology in imbibition and drainage for both wetting and nonwetting phases. The connected pathways of both wetting and nonwetting phases show however insignificant hysteresis in the topology in drainage and the imbibition. Therefore, the hysteresis is likely to be caused by the ganglia part of the phases.
- The topology change in the wetting connected pathway (χ_{wP}) seems to be dictated by the pore geometry and the wetting changes. The topology of the connected pathway of the wetting phase due to its affinity to rock may not change much unless the affinity itself (wettability) has changed.
- Less dependency of the nonwetting phase topology on the pore geometry makes the nonwetting phase topology a suitable criterion to study the displacement process (reported also by Schlüter et al. 2016).
- The ratio of the Euler characteristic for connected pathways of wetting (water) and nonwetting (oil) phases seems to be a descriptor of the wetting change.

ACKNOWLEDGEMENT

The experiment was performed at the TOMCAT beamline in the Swiss Light Source, *Paul Scherrer Institute*. We thank Morten Vassvik and Reidun Cecilie Aadland for help in performing the experiment, and Per Arne Slotte and Carl Fredrik Berg for discussions. This

work was partly supported by the *Research Council of Norway* through *Centers of Excellence* funding scheme, project no. 262644.

REFERENCES

1. Armstrong, RT, JE McClure, MA Berrill, M Rücker, S Schlüter, S Berg, "Beyond Darcy's law: The role of phase topology and ganglion dynamics for two-fluid flow," Physical Review E, (2016) 94, 043113, 1–10.
2. Armstrong, RT, JE McClure, MA Berrill, M Rücker, S Schlüter, S, Berg, "Flow Regimes During Immiscible Displacement," Petrophysics, (2017) Feb, 58 (1), 10–18.
3. Avraam, DG, AC Payatakes, "Flow regimes and relative permeabilities during steady-state two-phase flow in porous media," J. Fluid Mech., (1995) 293, 207–236.
4. Bartels, WB, H Mahani, S Berg, R Menezes, JA van der Hoeven, A Fadili, "Oil Configuration Under High-Salinity and Low-Salinity Conditions at Pore Scale: A Parametric Investigation by Use of a Single-Channel Micromodel," Society of Petroleum Engineers (SPE), SPE Journal (2017a) Feb.
5. Bartels, WB, M Rücker, S Berg, H Mahani, A Georgiadis, A Fadili, N Brussee, A Coorn, H van der Linde, C Hinz, A Jacob, C Wagner, S Henkel, F Enzmann, A Bonnin, M Stampanoni, H Ott, M Blunt, SM Hassanizadeh, "Fast X-Ray Micro-CT Study of the Impact of Brine Salinity on the Pore-Scale Fluid Distribution During Waterflooding," Petrophysics, (2017b) Feb, 58 (1), 36–47.
6. Berg, S, RT Armstrong, A Georgiadis, H Ott, A Schwing, R Neiteler, N Brussee, A Makurat, M Rücker, L Leu, M Wolf, F Khan, F Enzmann, M Kersten, "Onset of Oil Mobilization and Nonwetting-Phase Cluster-Size Distribution," Petrophysics, (2015) Feb, 56 (1), 15–22.
7. Doube, M, MM Kłosowski, I Arganda-Carreras, F Cordeliéres, RP Dougherty, J Jackson, B Schmid, JR Hutchinson, SJ Shefelbine, "BoneJ: Free and extensible bone image analysis in ImageJ," Bone, (2010) 47:1076–9.
8. Herring, AL, EJ Harper, L Andersson, A Sheppard, BK Bay, D Wildenschild, "Effect of fluid topology on residual nonwetting phase trapping: Implications for geologic CO_2 sequestration," Adv. Water Resour. (2013) 62, 47–58.
9. Khanamiri, HH, M Nourani, T Tichelkamp, JÅ Stensen, G Øye, O Torsæter, "Low salinity surfactant EOR with a new surfactant blend: effect of calcium cations," *Energy & Fuels*, (2016a) 30 (2), 984–991.
10. Khanamiri, HH, O Torsæter, JÅ Stensen, "Effect of Calcium in Pore Scale Oil Trapping by Low-Salinity Water and Surfactant Enhanced Oil Recovery at Strongly Water-Wet Conditions: In Situ Imaging by X-ray Microtomography," *Energy & Fuels*, (2016b) *30* (10), 8114–8124.
11. Münch, B; Xlib, http://imagej.net/Xlib, 2015.
12. Nock, R, F Nielsen, "Statistical Region Merging," IEEE Trans. Pattern Anal. Mach. Intell. (2004) 26 (11): 1452–1458.
13. Rücker, M, S Berg, RT Armstrong, A Georgiadis, H Ott, A Schwing, R Neiteler, N Brussee, A Makurat, L Leu, M Wolf, F Khan, F Enzmann, M Kersten, "From connected pathway flow to ganglion dynamics," Geophys. Res. Lett. (2015) 42, 3888–3894.
14. Schlüter, S, S Berg, M Rücker, RT Armstrong, HJ Vogel, R Hilfer, D Wildenschild, "Pore-scale displacement mechanisms as a source of hysteresis for two-phase flow in porous media," Water Resour. Res. (2016), 52, 2194–2205.
15. Tsai, W, "Moment-preserving thresholding: a new approach," Computer Vision, Graphics, and Image Processing, (1985) 29: 377–393.
16. Tschmperlé, D, R Deriche, "Vector-Valued Image Regularization with PDE's: A Common Framework for Different Applications," IEEE Trans. Pat. Anal. Mach, Intell. (2005) 27 (4): 506–517.
17. Youssef, S, E Rosenberg, H Deschamps, R Oughanem, E Maire, R Moks, "Oil ganglia dynamics in natural porous media during surfactant flooding captured by ultra-fast x-Ray microtomography," International Symposium of the Society of Core Analysts, SCA2014-23, Sep (2014), Avignon, France.